Dissimilar Laser Welding/Brazing of 5754 Aluminum Alloy to DP 980 Steel: Mechanical Properties and Interfacial Microstructure

JIN YANG, YULONG LI, HUA ZHANG, WEI GUO, DAVID WECKMAN, and NORMAN ZHOU

A diode laser welding/brazing technique was used for lap joining of 5754 aluminum alloy to DP 980 steel with Al-Si filler metal. The correlation between joint interfacial microstructure, wettability of filler metal, and mechanical properties was systematically investigated. At low laser power (1.4 kW), a layer of intermetallic compounds, composed of θ-Fe(Al,Si)$_3$ and τ_5-Al$_{7.2}$Fe$_{1.8}$Si, was observed at the interface between fusion zone and steel. Because of the poor wettability of filler metal on the steel substrate, the joint strength was very low and the joint failed at the FZ/steel interface. When medium laser power (2.0 kW) was applied, the wettability of filler metal was enhanced, which improved the joint strength and led to FZ failure. With further increase of laser power to 2.6 kW, apart from θ and τ_5, a new hard and brittle η-Fe$_2$(Al,Si)$_5$ IMC with microcracks was generated at the FZ/steel interface. The formation of η significantly degraded the joint strength. The failure mode changed back to interfacial failure.

DOI: 10.1007/s11661-015-3079-x

I. INTRODUCTION

LIGHTWEIGHT alloys have been increasingly applied in fabricating automotive and aerospace body structures and skin panels to enhance the fuel efficiency, improve the operating range, and decrease greenhouse gas emission.[1–3] Among various lightweight alloys, aluminum alloys are among the most popularly used materials due to their low density, good workability, and recyclability, as well as superior corrosion resistance. Therefore, many conventional all-steel body structures nowadays have been replaced by steel and aluminum parts, making joining of aluminum to steel inevitable.

Although aluminum/steel dissimilar joints have been widely applied, joining of aluminum to steel is still a challenge due to their huge disparity in physical properties[4,5] and rapid formation and growth of Fe-Al intermetallic compounds (IMCs). Fe-Al IMCs can significantly embrittle the joint because of their low critical stress intensity factor and high crack propagation rate.[6] Therefore, the main issue of joining of aluminum to steel is to control the formation and growth of the Fe-Al IMCs. To date, many joining technologies have been used to join aluminum to steel. Solid-state welding is a promising method as the formation and growth of Fe-Al IMCs can be significantly limited by avoiding the melting of parent metals.[7–9] However, the shape and size of joint are extremely restricted by the capacity of welding equipment. To avoid these issues of solid-state welding, hybrid welding/brazing is being considered because it creates a fusion welding joint at the aluminum side and a brazing joint at the steel side. In this kind of joining technology, various alloy elements, such as Si,[10–15] Zn,[16–19] Cu,[20,21] and Mg,[22] are used in filler metals in order to suppress the formation and growth of Fe-Al IMCs. Among those alloy elements, Si has been regarded as an effective element to limit the thickness of IMCs layer by decreasing the diffusion rate of Al through the IMC layer and favoring the dissolution of the IMC layer.[23–26] Song *et al.*[10,15] observed that θ-Fe(Al,Si)$_3$ was formed before τ_5-Al$_{7.2}$Fe$_{1.8}$Si in the reaction layer in arc welded/brazed aluminum-steel joints with Al-Si-based filler metals. Mathieu *et al.*[11] and Saida *et al.*[12] optimized the process parameters in laser joining of aluminum to steel with Al-Si filler metal. Su *et al.*[13] quantitatively analyzed the pores in the resolidified Al-Si melt pool in arc welded/brazed aluminum-steel joints. However, most of the literature has mainly focused on the formation sequence of IMCs, process parameter optimization, and defect analysis. There is little work on the correlation between joint interfacial microstructure and mechanical properties.

JIN YANG, PhD Candidate, is with the Key Lab of Robot and Welding Automation of Jiangxi Province, School of Mechanical and Electrical Engineering, Nanchang University, Nanchang, Jiangxi 330031, China, and also with the Center for Advanced Materials Joining, University of Waterloo, Waterloo, ON N2L 3G1, Canada. Contact e-mails: mryoung789@gmail.com and zhanghua_dr@163.com YULONG LI and HUA ZHANG, Professors, are with the Key Lab of Robot and Welding Automation of Jiangxi Province, School of Mechanical and Electrical Engineering, Nanchang University. WEI GUO, Professor, is with the School of Mechanical Engineering and Automation, Beijing University of Aeronautics and Astronautics, Beijing 100191, China. DAVID WECKMAN and NORMAN ZHOU, Professors, are with the Center for Advanced Materials Joining, University of Waterloo.

Manuscript Submitted December 16, 2014.
Article published online July 28, 2015

In this work, diode laser welding/brazing technology was used to join aluminum alloy to steel with Al-Si filler metal over a wide range of laser powers. The aim of the study was to investigate the correlation between joint interfacial microstructure and mechanical properties. The influence of wettability of filler metal on the joint strength is also discussed.

II. EXPERIMENTAL PROCEDURES

Zn-coated DP980 steel sheet in a thickness of 1.0 mm was used in the present study. The zinc coating was obtained by hot dip galvanizing with the thickness of 10 to 15 μm. 2-mm-thick AA 5754-O Al-Mg alloy was used. 4047 filler metal (Al-12Si) with the diameter of 1.6 mm was used. The chemical compositions and mechanical properties of the materials are given in Tables I and II, respectively. An anticorrosive brazing flux Superior No. 20 manufactured by Superior Flux and Manufacturing Co. was used. This powder flux was composed of LiCl (30 to 45 wt pct), KCl (30 to 45 wt pct), NaF (10 to 25 wt pct), NaCl (8 to 13 wt pct), and $ZnCl_2$ (6 to 10 wt pct). The as-received powder flux was mixed with ethanol into a paste and then evenly sprinkled on the sample to obtain an estimated average thickness of 10 to 50 μm.

The DP980 steel and 5754 aluminum alloy coupons were cut to the dimensions of 50 mm × 60 mm. All specimens were sheared to size parallel to the rolling direction. Prior to welding, DP980 steel and 5754 aluminum alloy were cleaned using acetone and methanol. The 5754 aluminum alloy was then immersed in a 10 to 15 pct NaOH solution heated to 333 K to 343 K (60 °C to 70 °C) for 2 to 3 minutes, rinsed with cold water, immersed in a 30 pct HNO_3 solution for 1 to 2 minutes, rinsed with hot water, dried, and then manually stainless steel wire brushed.

Diode laser welding/brazing experiments were performed with a Nuvonyx diode laser system (maximum power of 4.0 kW) and a Panasonic six-axis robot arm. The intensity distribution of the laser beam at the focal point was rectangular in shape (1 mm × 12 mm) with a uniform intensity profile. The filler metal was preset on the surface of the steel sheet. In order to limit oxidation, argon shielding gas was provided with a flow rate of 15 L/minute from a 6-mm-diameter flexible copper feeding tube. A shim with the same thickness as the steel sheet was used underneath the aluminum alloy side to control the gaps between the faying surfaces. The layout of laser welding/brazing experiment is illustrated in Figure 1(a). The process parameters were 1.0 to 2.8 kW laser power and 1.0 m/minute travel speed, with the laser beam focused on top of the filler metal.

Tensile test specimens with dimensions of 50 mm × 3.5 mm were cut from the assemblies by the abrasive water jet technique. The specimens were evaluated by tensile-shear tests at room temperature with a crosshead speed of 1 mm/minute using Instron 5548 Micro Tester, in a direction perpendicular to the joining line, as shown in Figure 1(b). Shims were used at each end of the specimens to ensure shear loads in the overlap joint while minimizing induced couples or bending of the specimens. The joint strength is presented in N/mm (failure load divided by tensile specimen width) as the geometry of the tensile specimens was not identical due to different FZ geometries developed in laser welding/brazing under different process conditions

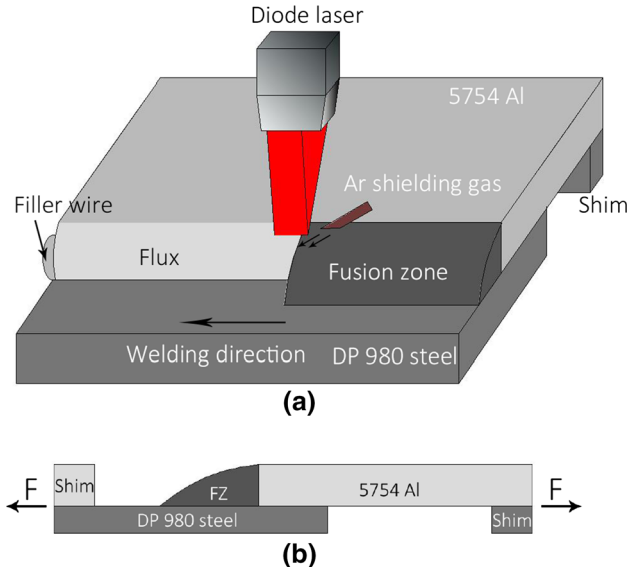

Fig. 1—(*a*) Schematic description of the laser welding/brazing layout used for joining the aluminum alloy to steel sheets in the lap joint configuration and (*b*) schematic illustration of the tensile-shear test samples.

Table I. Chemical Composition of the Materials in Weight Percent

Materials	Mg	Cr	Mn	Si	Cu	Zn	Ti	Fe	Mo	C	Al	B
DP 980	—	0.15	2.1	0.05	—	—	—	bal.	0.35	0.135	0.45	0.007
5754 Al	2.6 to 3.6	0.3	0.5	0.4	0.1	0.2	0.15	0.4	—	—	bal.	—
4047 Al	0.1	—	0.01	11.9	0.05	0.01	—	0.17	—	—	bal.	—

Table II. Mechanical Properties of the Base Materials

Materials	Yield Strength (MPa)	Ultimate Strength (MPa)	Elongation (Pct)
DP 980	666 ± 36	1005 ± 7	12.5 ± 0.7
Al 5754	85 ± 11	239 ± 3	16.2 ± 1.3

and the complex stresses involved in such situations.[27] Nanohardness of the IMC was evaluated using a Hysitron TriboIndenter with a constant force of 4 mN.

After welding, specimens were cut from the laser joints and mounted in phenolic resin. The specimens were then mechanically ground using 400, 600, 800, 1000, and 1200 grades of SiC papers followed by polishing with a 1 μm diamond suspension. They were then etched in Keller's reagent (1 mL HCl, 1.5 mL HNO_3, 2.5 mL HF, and 95 mL H_2O) for 3 to 5 seconds to reveal the microstructure. The microstructure and fracture morphology were analyzed using a JEOL JSM 6460 scanning electron microscope (SEM) with operating 20 kV voltage equipped with Oxford INCA energy-dispersive X-ray spectrometer (EDS). The FZ/steel interfacial phases were confirmed using a JEOL 2010F transmission electron microscope (TEM). The phase constitution of fractured joints was analyzed by X-ray diffraction (XRD) using an INEL XRG-3000 diffractometer with Cu Kα1 radiation (wavelength λ = 1.5406 Å) at 30 kV and 30 mA.

III. RESULTS

A. *Microstructures*

Figure 2(a) shows a typical weld cross section of the laser joint. During laser irradiation, filler metal melted, wetted, and spread on the steel surface, then solidified to form the FZ. In order to characterize the wettability of filler metal on the steel substrate, the FZ geometry was investigated. The brazed width and wetting angle were measured using the definitions illustrated in Figure 2(a). Figure 2(b) shows the change of brazed width and wetting angle with respect to the laser power. As shown, the brazed width increased with rising laser power, while wetting angle decreased with the increase of laser power. The increased brazed width and decreased wetting angle indicate an improved wettability of filler metal. This improvement is apparently due to the fact that the surface tension and viscosity of molten filler metal decrease with the increase of laser heat input.[28] It in turn has an influence on the joint strength, as indicated in the literature,[29,30] which will be discussed later.

Figure 3(a) presents the interfacial microstructure of laser joint with low laser power (1.4 kW). Two distinct IMCs were observed at the FZ/steel interface. To analyze the IMCs, EDS point analysis was performed at zones A and B (Table III). According to the Fe-Al-Si phase diagram,[31,32] the possible phases of IMCs are τ_5-$Al_{7.2}Fe_{1.8}Si$ and θ-$Fe(Al,Si)_3$. The IMCs were then confirmed by TEM and XRD as discussed later. As shown in Figure 3(a), τ_5 presents an island-shaped structure at the FZ side, while θ appears to be bumpy at the steel side. Figure 4(a) shows the TEM image of the FZ/steel interface. As shown in Figure 4(a), a continuous IMC layer composed of two phases is observed at the FZ/steel interface. The selected area diffraction patterns (SADPs) (Figures 4(b) and (c)) represent the incident beams parallel to $[\bar{1}2\bar{1}1]_{\tau_5}$ and $[0\bar{2}1]_{\theta}$ zone axes which confirms the phases identified by the EDS analysis.

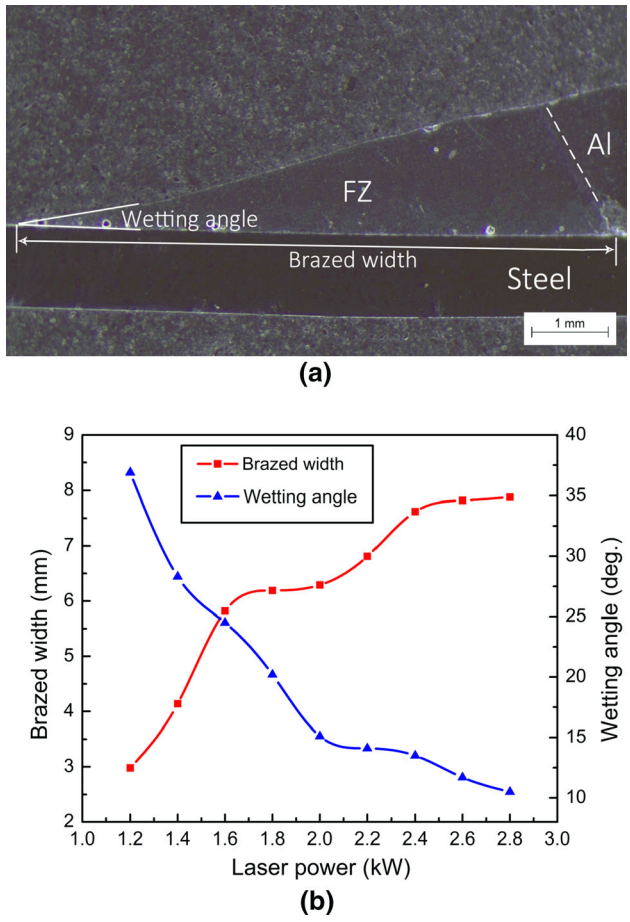

Fig. 2—(*a*) Typical cross section of the laser dissimilar joint between aluminum alloy and steel and (*b*) laser power *vs* brazed width and wetting angle.

The interfacial microstructure of laser joint with medium laser power (2.0 kW) is shown in Figure 5(a). Similar to low laser power, two distinct IMCs were observed at the FZ/steel interface. Based on EDS analysis at zones C and D (Table III), τ_5 and θ were identified. As shown, the morphology of θ changed from bumpy into needle like which was approximately perpendicular to the FZ/steel interface. Meanwhile, τ_5 changed from island shaped to scallop like. The formation and growth of IMCs are mainly controlled by Fe atom diffusion and dissolution from steel toward FZ during laser irradiation.[11,18,33] Thus, the change of interfacial microstructure can be understood as described below. Compared to the low laser power, higher maximum temperature and longer time for Fe atom diffusion and dissolution toward the FZ could be attained, and therefore higher Fe content can be attained at the FZ/steel interface at medium laser power. This will lead to a stronger metallurgical reaction and results in the change of interfacial microstructure. The evidence can be reviewed by comparing EDS line scan profiles of low and medium laser powers (Figures 3(b) and 5(b)). It was found that the diffusion distance of Fe atom increased from 3.5 to 5 μm, and the thickness of diffusion layer (DL) increased from 0.5 to

0.7 μm. The DL is rich in elements Fe and Al, which is confirmed as Fe(Al) solid solution by SADP (Figure 4(d)). Ali[34] has also reported the Fe(Al) diffusion layer at the steel side in laser brazed steel/Mg-Al joints.

Figure 6(a) shows a typical interfacial microstructure of laser joint with high laser power (2.6 kW). In comparison with low and medium laser powers, a prominent change in the interfacial microstructure occurred. In addition to θ and τ_5, a new planar IMC with microcracks was observed at the interface. Based on EDS analysis at zones G (Table III), the possible phase of new IMC is η-$Fe_2(Al,Si)_5$. Furthermore, the morphology of θ and τ_5 changed into rod shaped and irregular polygon shaped, respectively. Since higher maximum temperature and longer time for Fe atom diffusion and dissolution can be attained at high laser power, η could form at the interface. The EDS line scan (Figure 6(b)) shows further evidence of this effect, where the longest diffusion distance of Fe atoms (11.5 μm) and thickest DL (1 μm) are shown. Song *et al.*[10,15] and Mei *et al.*[35] observed only θ and τ_5 at the FZ/steel interface of welded/brazed aluminum/steel joint, which is similar to the joint obtained with low and medium laser powers in this study. The absence of η is expected to result from insufficient heat input and insufficient diffusion and dissolution of Fe atoms. It is of interest to observe that η appears to be planar rather than having a tongue-like or saw-tooth morphology,[36] which is due to its sluggish growth caused by the occupation of vacancy sites by Si atoms.[37]

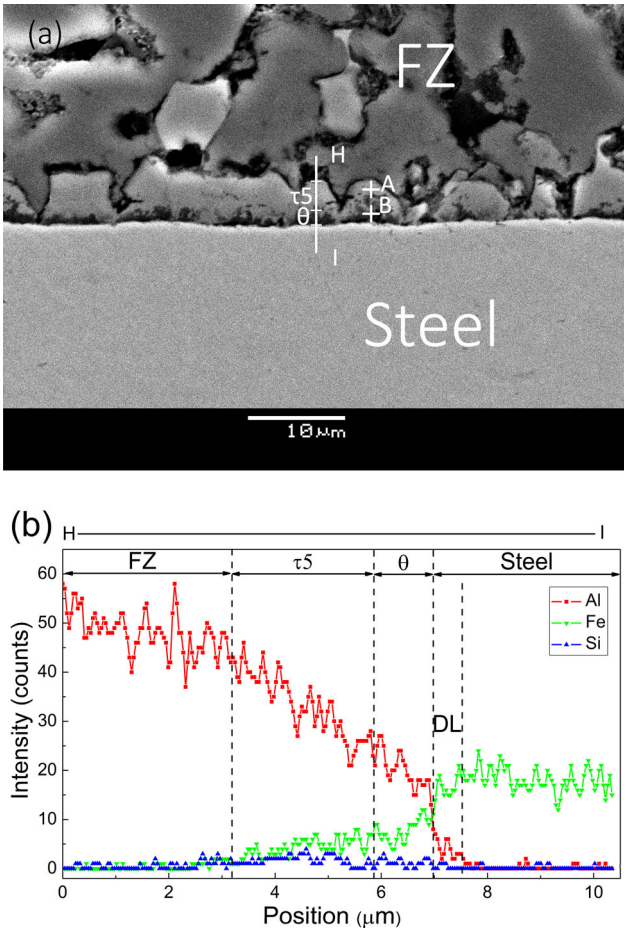

Fig. 3—(*a*) SEM image of the FZ/steel interface at 1.4 kW laser power and (*b*) EDS line scan along the line HI in (a).

B. *Mechanical Properties*

The joint strength is displayed as a function of the laser power in Figure 7. The joint strength increased progressively with the increase of laser power ranging from 1.2 to 1.6 kW. In that power range, the failure mode was interfacial at the FZ/steel interface. Then, a maximum plateau was attained at laser powers of 1.8 to 2.0 kW, which led to an FZ failure at the Al/FZ interface. However, the joint strength then decreased with the further increase of laser power (2.2 to 2.8 kW), and the failure mode changed back to interfacial failure at the FZ/steel interface.

The changes of joint strength and fracture behavior can be correlated to the change of interfacial microstructure and wettability of filler metal. When laser power was lower than 1.8 kW, the increase of joint strength was mainly ascribed to the enhancement of wettability of filler metal (Figure 2(b)). This is because the effective bonding area increased with the increase of wettability. When the laser power was between 1.8 and 2.0 kW, the bonding strength at the FZ/steel interface exceeded the bonding strength at the Al/FZ interface, which caused the change in failure mode. When laser power was higher than 2.0 kW, the decrease of joint strength was attributed to the formation of hard and brittle IMC η (Figure 8) as well as the microcracks, even though the wettability of filler metal was improved.

C. *Fractography*

Figure 9 shows the schematic illustrations, SEM images of fracture surfaces, and XRD analysis of failure

Table III. EDS Analysis of the Marked Zones in Figs. 3(a), 5(a), and 6(a) in Atomic Percent

Zones	Al	Si	Fe	Possible Phases
A	74.6 ± 1.0	7.8 ± 0.4	17.6 ± 0.9	τ_5-$Al_{7.2}Fe_{1.8}Si$
B	69.9 ± 2.4	4.5 ± 0.7	25.6 ± 2.6	θ-$Fe(Al,Si)_3$
C	73.5 ± 1.2	8.1 ± 1.7	18.4 ± 1.9	τ_5-$Al_{7.2}Fe_{1.8}Si$
D	71.7 ± 1.0	4.9 ± 0.8	23.4 ± 0.2	θ-$Fe(Al,Si)_3$
E	74.2 ± 2.7	7.5 ± 2.1	18.3 ± 2.9	τ_5-$Al_{7.2}Fe_{1.8}Si$
F	70.0 ± 1.1	4.1 ± 0.4	25.9 ± 1.5	θ-$Fe(Al,Si)_3$
G	66.3 ± 1.6	4.3 ± 0.9	29.4 ± 1.0	η-$Fe_2(Al,Si)_5$

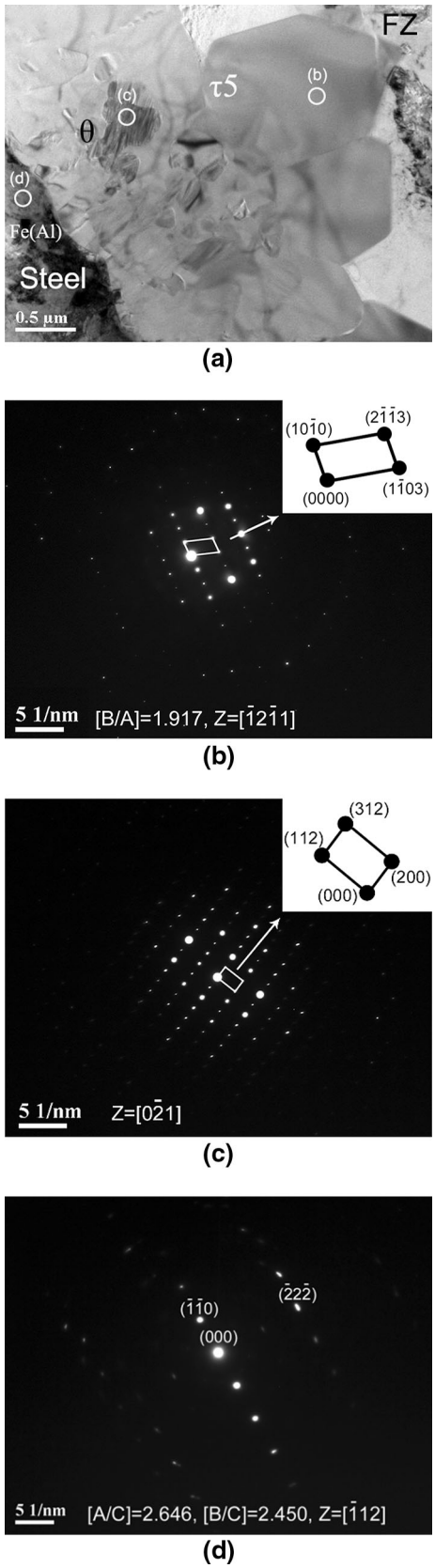

Fig. 4—(*a*) TEM image of the FZ/steel interface at 1.4 kW laser power and selected area electron diffraction patterns (SADPs) for (b) τ_5, (c) θ, and (d) Fe(Al) indicated in (a).

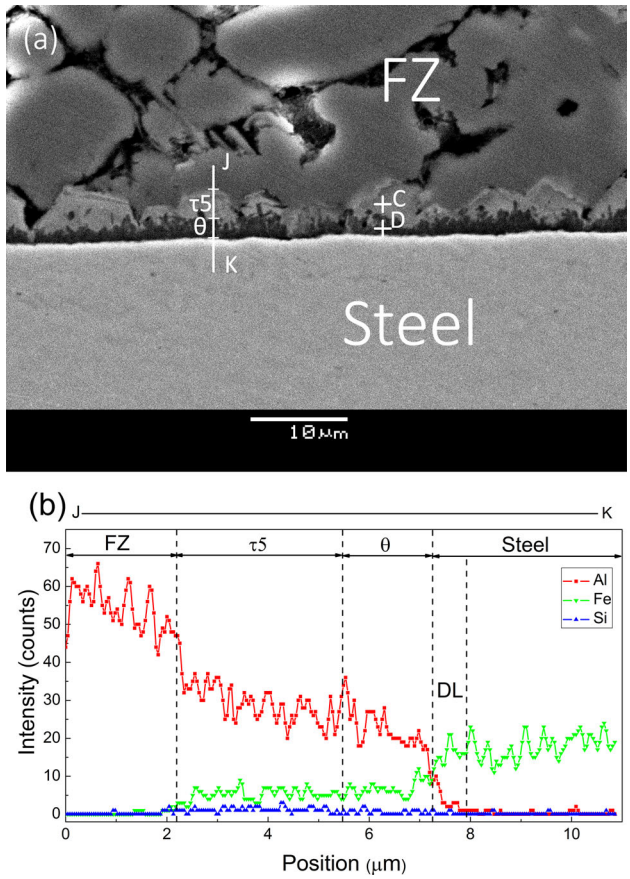

Fig. 5—(*a*) SEM image of the FZ/steel interface at 2.0 kW laser power and (*b*) EDS line scan along the line JK in (a).

joint with low laser power. As shown in Figures 9(c) and (d), typical brittle fracture surfaces with smooth planes were observed. Based on the EDS analysis, θ and τ_5 were determined on the fracture surfaces, which were confirmed by XRD analysis (Figure 9(e)). The brittle failure of joint was mainly induced by the hard and brittle nature of the IMCs formed at the FZ/steel interface.

Figure 10 displays the schematic illustrations and SEM images of fracture surfaces of failure joint with medium laser power. As shown, a mixture of smooth planes and river patterns were seen on the fracture surface which is characteristic of brittle cleavage failure. In addition to α-Al and Al-Si eutectic (Figures 10(c) and (e)), some platelet structures were visible on the fracture surface, as displayed in Figures 10(d) and (f). According to the EDS analysis, the Fe-Al-Si ternary alloy phase diagram, and typical characteristics of Fe-Al-Si systems,[31,32] the possible phase of platelet-shaped structure is τ_6-Al_5FeSi. It is a kind of IMC with sharp edges which could induce severe stress concentration and result in brittle failure of the joint.[15]

Figure 11 shows the schematic illustrations, SEM images of fracture surfaces, and XRD analysis of the failure joint with higher laser power. Again, it was determined as brittle fracture due to the smooth planes shown on the fracture surfaces (Figures 11(c) and (d)).

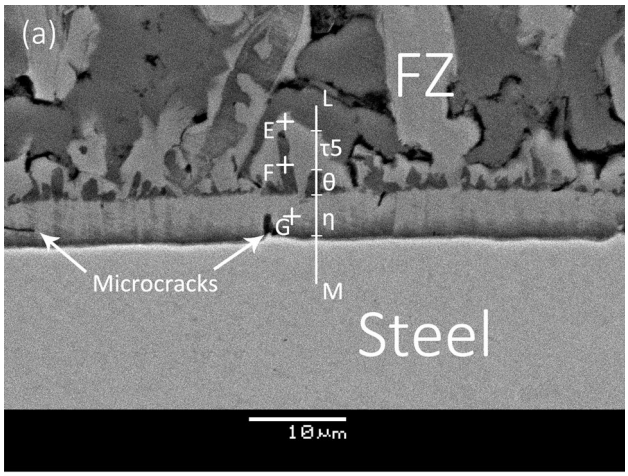

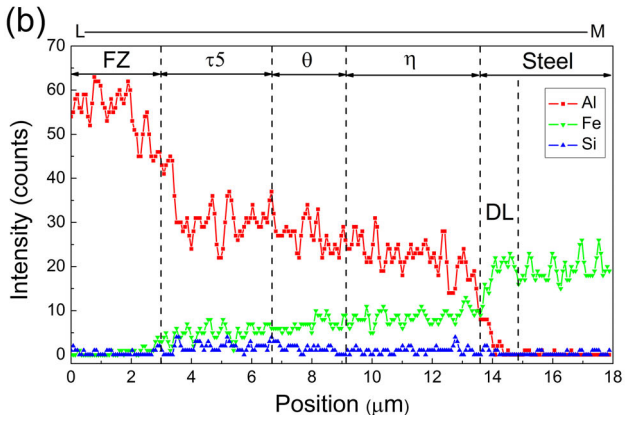

Fig. 6—(*a*) SEM image of the FZ/steel interface at 2.6 kW laser power and (*b*) EDS line scan along the line LM in (a).

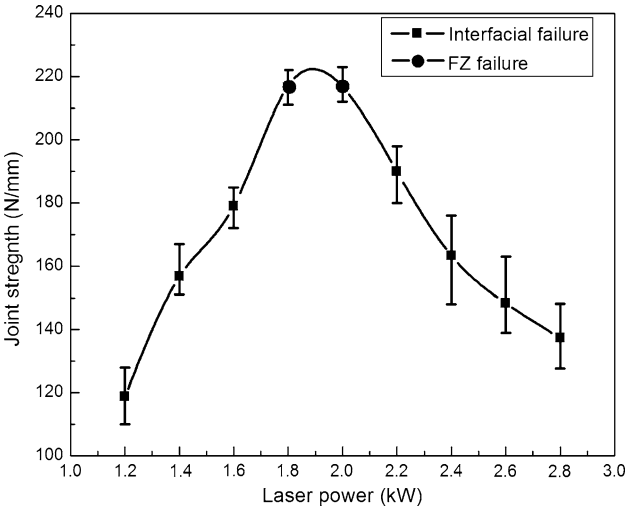

Fig. 7—Laser power *vs* joint strength showing the joint failure modes.

EDS analysis showed that only η was found on the fracture surfaces. Figure 11(e) displays the XRD pattern from the fractured surface at the FZ side. The peaks of τ_5 were detected due to the fact that X-ray is able to reveal the diffraction pattern of substance located several microns underneath the detected surface. In the present study, the penetration depth was calculated to be around 18.2 to 20.6 μm at 2θ from 42 to 48 deg, where was the location for the majority of IMCs peaks.[38–40] While, the absence of θ peaks may be because they were too low in quantity to be detected. Basically, these findings are consistent with the SEM and EDS analyses. It was determined that the crack propagates only through η, owing to its highest hardness among the IMCs.

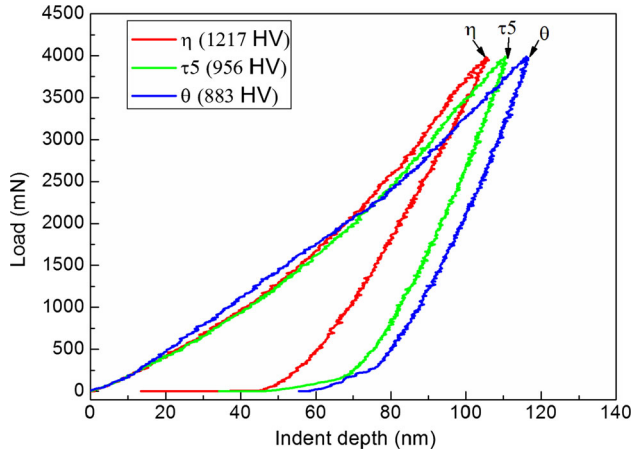

Fig. 8—Load *vs* indent depth indicating nanohardnesses of the IMCs.

IV. DISCUSSION

From the above results, the evolution of interfacial phases with the increasing laser power can be explained as follows. In order to clarify the process, it is of importance to know the sequence of phase formation during the solidification. Song *et al.*[10] and Viala *et al.*[25] both pointed out that θ was formed before τ_5. Mei *et al.*[35] revealed that τ_5 had higher thermodynamic stability than η, and therefore τ_5 would be formed before η. Besides, in Reference 36, it was mentioned that θ was formed before η. Therefore, it is reasonable to determine that the sequence of phase formation is θ, τ_5, and η. A schematic diagram is provided to assist the following discussion (Figure 12).

At low and medium laser powers, the liquid filler metal wets and spreads on the solid steel substrate. Fe atoms diffuse and dissolve into the FZ until the concentration of Fe atom increases to saturation concentration. Meanwhile, Si atoms in the FZ tend to aggregate at the FZ/steel interface.[10] Then, bumpy θ is formed at the solid–liquid interface between DL and FZ. The chemical reaction at the interface can be represented as $L \rightarrow L' + \theta$.[10] During the solidification process, island-shaped τ_5 is then generated between θ and FZ (Figure 12(a)) due to the phase transformation $L + \theta \rightarrow \tau_5$.[25]

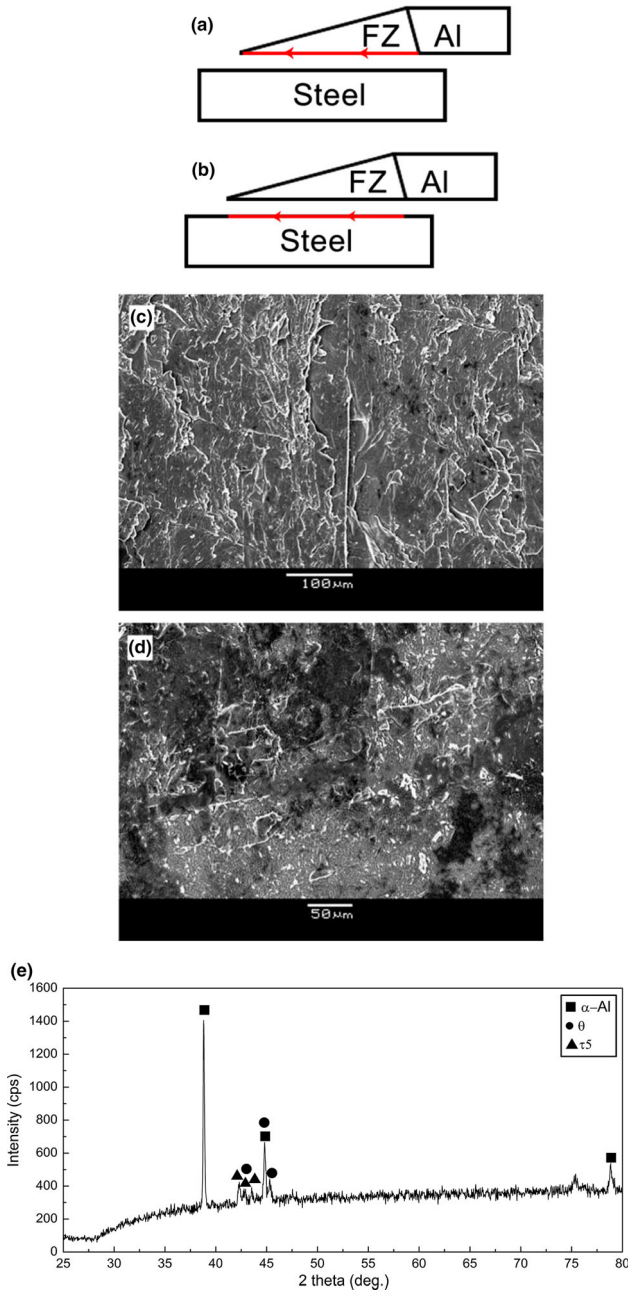

Fig. 9—Fracture surfaces and XRD analysis of the joint with low laser power: (*a*) and (*b*) schematic diagrams of the fracture locations showing the fracture directions by arrows, (*c*) SEM image of the fracture surface at FZ side, (*d*) SEM image of the fracture surface at the steel side, and (*e*) XRD patterns of the fracture surface at the FZ side.

At high laser power, a continuous IMC layer, composed of θ and τ_5, is generated first, which followed by the formation of η at the interface between steel and θ. The chemical reaction is through a solid–solid reaction, which can be expressed as $\theta + \mathrm{Fe} \rightarrow \eta$.[36] The formation of η is ascribed to the diffusion of Fe atoms toward the interface. Since η is extremely hard and brittle, microcrack is easy to initiate and propagate in the phase during the cooling (Figure 12(b)).

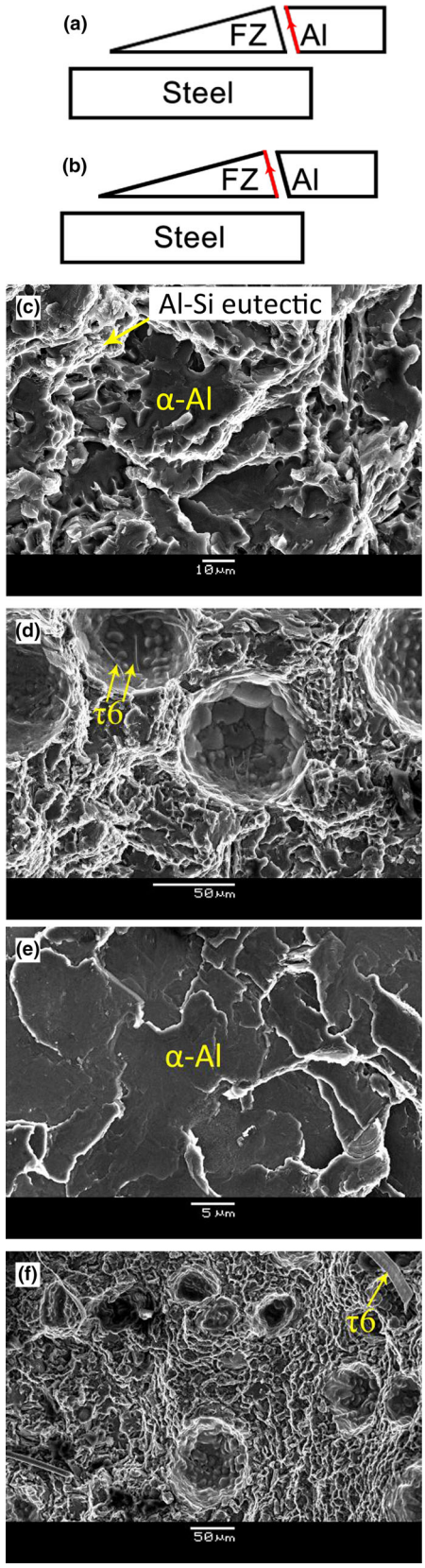

Fig. 10—Fracture surfaces of the joint with medium laser power: (*a*) and (*b*) schematic diagrams of the fracture locations showing the fracture directions by arrows, (*c*) and (*e*) SEM images of the fracture surface at the Al side, and (*d*) and (*f*) SEM images of the fracture surface at the FZ side.

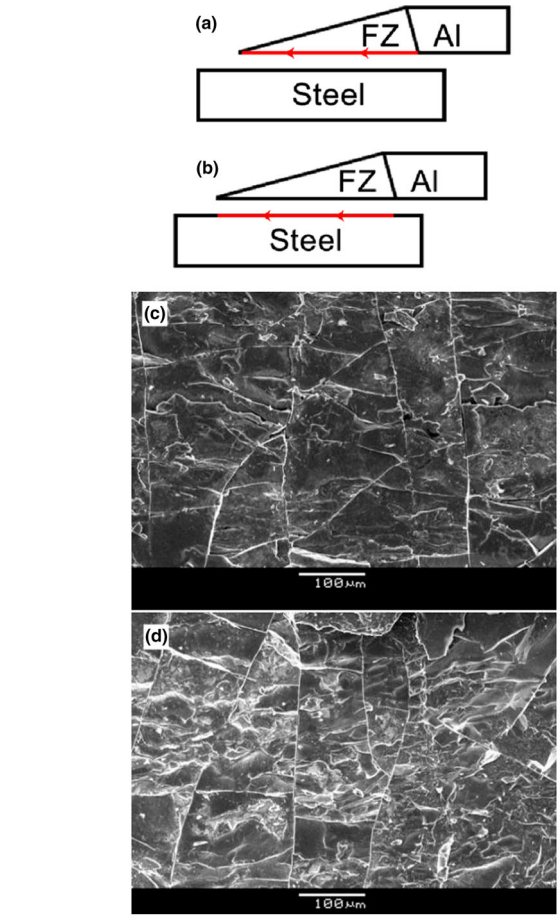

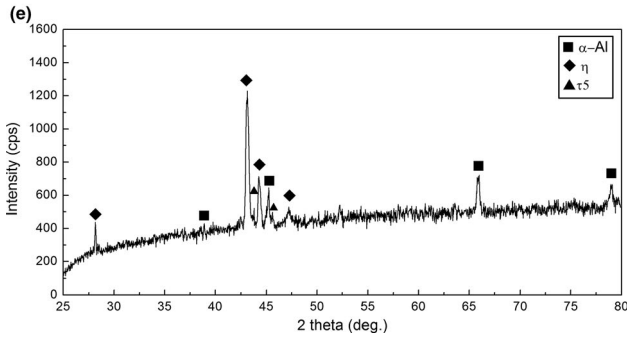

Fig. 11—Fracture surfaces and XRD analysis of the joint with high laser power: (*a*) and (*b*) schematic diagrams of the fracture locations showing the fracture directions by arrows, (*c*) SEM image of the fracture surface at the FZ side, (*d*) SEM image of the fracture surface at steel side, and (*e*) XRD patterns of the fracture surface at the FZ side.

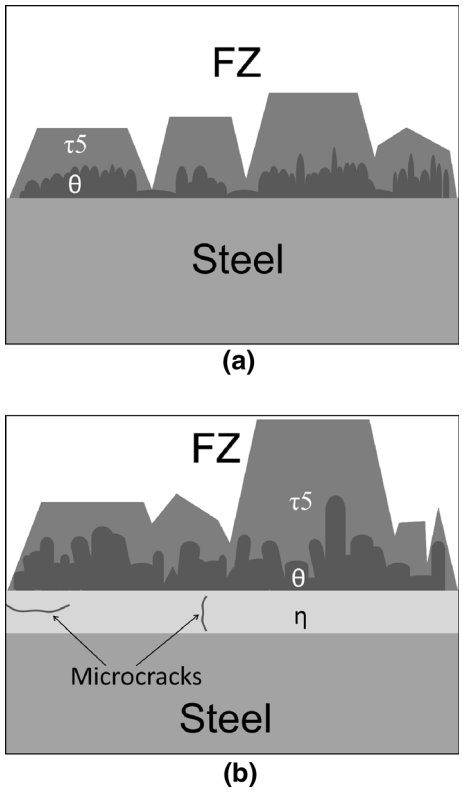

Fig. 12—Schematic illustration of the evolution of interfacial phases with increasing laser power: (*a*) low and medium laser powers and (*b*) high laser power.

V. CONCLUSIONS

Dissimilar joining of aluminum alloy to steel was achieved successfully by laser welding/brazing using Al-Si filler metal over a wide range of laser powers. The correlation between interfacial microstructure, wettability of filler metal, and joint mechanical property was systematically investigated. The major conclusions can be summarized as follows:

1. At low laser power, a continuous IMC layer, composed of θ and τ_5, is formed at the FZ/steel interface. Because of low laser heat input, the resultant wettability of filler metal is poor. An unfavorable interfacial failure between θ and τ_5 with low joint strength is obtained.
2. At high laser power, a prominent change in the interfacial microstructure occurs. Apart from θ and τ_5, a hard and brittle η phase with microcracks is formed at the FZ/steel interface. Its formation mainly results from the diffusion of Fe atoms into θ in solid state. It significantly embrittles the joint, leading to a low joint strength and an interfacial failure through η, regardless of the improved wettability of filler metal.
3. At medium laser power, only θ and τ_5 are formed at the FZ/steel interface. The enhancement of wettability significantly improves the joint strength and results in a desirable FZ failure at the Al/FZ interface. Thus, laser power should be strictly controlled due to the competition between the poor wettability of filler metal at low laser power and the formation of η and microcracks at high laser power.

ACKNOWLEDGMENTS

Financial support of State Scholarship Fund of China (Grant No. 201306820002) and the National Natural Science Foundation of China (No. 51265035) is

gratefully acknowledged. The authors would like to thank Dr. A.M. Nasiri and PhD candidates H. Huang, D.C. Saha, and D. Xu from Centre for Advanced Materials Joining, University of Waterloo, for valuable discussions. The authors thank Dr. Yuquan Ding from the Materials Science and Engineering Group, University of Waterloo, for the help with SEM, EDS, and nanohardness operations. The TEM research was performed at the Canadian Centre for Electron Microscopy at McMaster University, which is supported by NSERC and other government agencies.

REFERENCES

1. K.H. Rendigs: *Mater. Sci. Forum*., 2008, vol. 242, pp. 11–24.
2. G.S. Cole and A.M. Sherman: *Mater. Charact*., 1995, vol. 35, pp. 3–9.
3. Y. Muraoka and H. Miyaoka: *J. Mater. Process Technol*., 1993, vol. 38, pp. 655–74.
4. M.J. Rathod and M. Kutsuna: *Weld. J*., 2004, vol. 83, pp. 16s–23s.
5. M.J. Torkamany, S. Tahamtan, and J. Sabbaghzadeh: *Mater. Des*., 2010, vol. 31, pp. 458–65.
6. V.X. Tran and J. Pan: *Int. J. Fatigue*, 2010, vol. 32, pp. 1167–79.
7. M. Acarer and B. Demir: *Mater. Lett*., 2008, vol. 62, pp. 4158–60.
8. M. Kimura, H. Ishii, M. Kusaka, K. Kaizu, and A. Fuji: *Sci. Technol. Weld. Join*., 2009, vol. 14, pp. 388–95.
9. M.S.A. Nezhad and A.H. Ardakani: *Mater. Des*., 2009, vol. 30, pp. 1103–09.
10. J.L. Song, S.B. Lin, C.L. Yang, and C.L. Fan: *J. Alloys Compounds*, 2009, vol. 488, pp. 217–22.
11. A. Mathieu, S. Pontevicci, J.C. Viala, E. Cicala, S. Matteï, and D. Grevey: *Mater. Sci. Eng. A*, 2006, vol. 435, pp. 19–28.
12. K. Saida, W. Song, and K. Nishimoto: *Sci. Technol. Weld. Join*., 2005, vol. 10, pp. 227–35.
13. Y. Su, X. Hua, and Y. Wu: *J. Mater. Process Technol*., 2014, vol. 214, pp. 81–86.
14. H.T. Zhang, J.C. Feng, P. He, and H. Hackl: *Mater. Charact*., 2007, vol. 58, pp. 588–92.
15. S.B. Lin, J.L. Song, C.L. Yang, and G.C. Ma: *Sci. Technol. Weld. Join*., 2009, vol. 14, pp. 636–39.
16. H. Dong, L. Yang, C. Dong, and S. Kou: *Mater. Sci. Eng., A*, 2010, vol. 527, pp. 7151–54.
17. A. Mathieu, R. Shabadi, A. Deschamps, M. Suery, S. Matteï, D. Grevey, and E. Cicala: *Opt. Laser Technol*., 2007, vol. 39, pp. 652–61.
18. G. Sierra, P. Peyre, F.D. Beaume, D. Stuart, and G. Fras: *Sci. Technol. Weld. Join*., 2008, vol. 13, pp. 430–37.
19. C. Dharmendra, K.P. Rao, J. Wilden, and S. Reich: *Mater. Sci. Eng. A*, 2011, vol. 528, pp. 1497–1503.
20. S.B. Lin, J.L. Song, C.L. Yang, C.L. Fan, and D.W. Zhang: *Mater. Des*., 2010, vol. 31, pp. 2637–42.
21. H. Dong, W. Hu, Y. Duan, X. Wang, and C. Dong: *J. Mater. Process Technol*., 2012, vol. 212, pp. 458–64.
22. Y. Su, X. Hua, and Y. Wu: *J. Mater. Process Technol*., 2014, vol. 214, pp. 750–55.
23. P. Vaillant and J.P. Petitet: *J. Mater. Sci*., 1995, vol. 30, pp. 4659–68.
24. M. Roulin, J.W. Luster, G. Karadeniz, and A. Mortensen: *Weld. J*., 1999, vol. 78, pp. 151s–55s.
25. J.C. Viala, M. Peronnet, F. Barbeau, F. Bosselet, and J. Bouix: *Compos. Part A App. Sci. Manuf*., 2002, vol. 33, pp. 1417–20.
26. D. Pierre, F. Barbeau, M. Peronnet, F. Bosselet, and J.C. Viala: *Defect Diffus. Forum*, 2001, vol. 194, pp. 1593–98.
27. S.H. Chen, J.H. Huang, K. Ma, X.K. Zhao, and A. Vivek: *Metall. Mater. Trans. A*, 2014, vol. 45A, pp. 3064–73.
28. D. Bonn, J. Eggers, J. Indekeu, J. Meunier, and E. Rolley: *Rev. Mod. Phys*., 2009, vol. 81, pp. 739–805.
29. H. He, C. Yang, S. Lin, C. Fan, Z. Chen, and Z. Chen: *Sci. Technol. Weld. Join*., 2014, vol. 19, pp. 527–33.
30. R. Kovacevic: *Welding Processes*, InTech, Croatia, 2012, pp. 33–54.
31. T. Maitra and S.P. Gupta: *Mater. Charact*., 2002, vol. 49, pp. 293–311.
32. Y. Li and B. Legendre: *J. Alloys Compd*., 2000, vol. 302, pp. 187–91.
33. A.M. Nasiri, L. Li, S.H. Kim, Y. Zhou, D.C. Weckman, and T.C. Nguyen: *Weld. J*., 2011, vol. 90, pp. 211s–19s.
34. A.M. Nasiri: PhD Dissertation, University of Waterloo, 2013.
35. S.W. Mei, M. Gao, J. Yan, C. Zhang, G. Li, and X.Y. Zeng: *Sci. Technol. Weld. Join*., 2013, vol. 18, pp. 293–300.
36. N. Takata, M. Nishimoto, S. Kobayashi, and M. Takeyama: *Intermetallics*, 2014, vol. 54, pp. 136–42.
37. W.J. Cheng and C.J. Wang: *Mater. Charact*., 2010, vol. 61, pp. 467–73.
38. B.D. Cullity: *Elements of X-Ray Diffraction*, 2nd ed., Addison-Wesley Publishing Co, Philippines, 1978, p. 135.
39. B.D. Cullity: *Elements of X-Ray Diffraction*, 2nd ed., Addison-Wesley Publishing Co, Philippines, 1978, p. 512.
40. Y.Y. Chang, C.C. Tsaur, and J.C. Rock: *Surf. Coat. Technol*., 2006, vol. 200, pp. 6588–93.